CITE this: Dalton trans. 2021

DOI: 10.1039/d1dt01519b

Heterometallic Co-Dy SMMs grafted on iron oxide nanoparticles

Lidia Rosado Piquer,[a],[c] Jan Dreiser,[b] and E. Carolina Sañudo[a],[c]*

[a] Department of Inorganic and Organic Chemistry, Inorganic Chemistry Section, Universitat de Barcelona; Carrer Martí i Franquès 1-11, 08028 Barcelona, Spain.

[b] Swiss Light Source, Paul Scherrer Institut, Forschungsstrasse 111, 5232 Villigen PSI, Switzerland

[c] Institut de Nanociència i Nanotecnologia IN2UB, Universitat de Barcelona, Carrer Martí i Franquès 1-11, 08028 Barcelona, Spain.

KEYWORDS (Word Style "BG_Keywords"). Iron oxide nanoparticles - 3d-4f SMMs - Van der Waals- surface functionalization - XMCD

ABSTRACT. The heterometallic 3d-4f SMM $[Co_4Dy(OH)_2(SALOH)_5(chp)_4(MeCN)(H_2O)_2]$ (**1**) has been deposited onto iron oxide nanoparticles (**NP**) with an oleate self-assembled monolayer (SAM) as surfactant. The hybrid molecular-inorganic system **1-NP** has been thoroughly characterized. The oleate SAM separates the SMM **1** from the magnetic substrate to avoid strong-coupling between surface and molecule to ensure that **1** retains its magnetic properties in **1-NP**. The magnetic properties of the hybrid system **1-NP** have been characterized by element specific XMCD: the heterometallic SMM retains its magnetic properties on the surface of the iron oxide NP while there is an enhancement of the magnetic properties of the **NP**s.

Introduction

In the 1990's the discovery of the possibility of a molecule to behave like a conventional magnet in the coordination complex $[Mn_{12}O_{12}(AcO)_{16}(H_2O)_4]$ by Sessoli[1] and Christou[2] was a turning point for molecular magnetism. These molecules were called single-molecule magnets (SMMs) and held the promise of new technologies, like using molecules for information storage, using quantum properties of SMMs for quantum information processing or using SMMs for molecular spintronic devices. The challenges for using molecules in devices were numerous, but from a basic point of view, the main shortcoming of SMMs is at present still the low temperature at which they can function. The energy barrier for the reversal of the magnetization (a combination of molecular magnetic moment and molecular anisotropy usually obtained from ac magnetic susceptibility measurements) in principle determines the blocking temperature: the higher the energy barrier the higher the blocking temperature should be. In practice, most SMMs display a plethora of 'under the barrier' relaxation processes, the most important of which is quantum tunneling of the

magnetization (QTM) that can result in the lack of a magnetic hysteresis opening. The main challenge remains to improve SMMs working temperatures. Several ideas have been proposed to overcome or improve this: exploiting the anisotropy of the lanthanide ions in 3d-4f complexes,[3] or controlling crystal field[4] around lanthanide ions to obtain SMMs with record energy barriers for the reversal of the magnetization.[5] The most successful examples have been delivered in the last five years. In 2016 Ruben and Dreiser showed how the true molecular hysteresis of the mononuclear SMM [$TbPc_2$][6,7] could be measured if isolated molecules were placed on a surface and decoupled from the surface phonons by an oxide layer.[8] They used a non-magnetic silver surface and the oxide was MgO. In 2017 and 2018, following his work on the topic of organometallic lanthanide SMMs[9,10] Layfield reported Dy metallocenium compounds that displayed hysteresis at 60 K[11] and 80 K.[12] Reta and Chilton offered theoretical insight on the high temperature hysteresis.[13] As Sessoli pointed out at the time, this put SMMs back in the race, showing that high-temperature hysteresis can be achieved for a molecular system.[14] These examples are both related to the fact that the relaxation of the magnetization is affected by factors not intrinsic to the SMM, but related to the environment of each individual molecule. Many researchers have proposed to use magnetic dilution, an SMM in a crystal of diamagnetic molecular analogues, to improve SMM properties.[15–18] Technologically it is still a challenge to address or manipulate single molecules, but an intermediate step could be the fabrication of nano-objects that contain a limited number of molecules, with defined sizes and that can be easily manipulated. One such nano-object is a hybrid SMM-iron oxide nanoparticle (NP). Iron oxide nanoparticles of 10-20 nm in diameters are superparamagnetic and easy to fabricate[19] and have many possible applications like easy catalyst recovery exploiting magnetic separation, drug and gene delivery, hyperthermia or even magnetic resonance imaging (MRI).[20–22,23] Core-shell nanoparticles can be

used to tailor the magnetic properties of the nanoobject or to maximize heat generation for magnetic hyperthermia.[24,25] Recent reports suggest that spin canting can play a very relevant role in the magnetic properties of the NP, and that this is particularly important for ultra-thin shells, where enhancement of the coercive field is observed.[26] In general it is accepted that if the shell is diamagnetic there will be little or no effect on the magnetic properties of the NP aside from a lowering of the saturation magnetization per gram of sample.[27] The effects of paramagnetic shells are not widely studied. Recently, Magnus and co-workers showed that magnetic order can be induced throughout a 40-nm-thick amorphous paramagnetic layer through proximity to ferromagnets, mediating both exchange-spring magnet behavior and exchange bias.[28] We already showed how such nano-objects can be prepared using either dopamine or SAM of oleate as buffer-layer between the NP and SMM.[29–31] Gold NP have been decorated with SMMs: the coordination bond between the NP surface and the SMM affects the magnetization relaxation properties of the SMM[32,33] showing the necessity to have an intermediate layer between SMM and surface. Similar results were reported Sessoli and co-workers, that observed a change in the relaxation dynamics of Fe_4 SMMs grafted onto Au NP.[34] Prado and co-workers reported that hysteresis of Fe_2O_3 NP is enhanced when coupled to a Co(II) complex.[35] Improvem

In the system presented here the $[Co_4Dy(OH)_2(SALOH)_5(chp)_4(MeCN)(H_2O)_2]$ (**1**)SMMs are separated from the iron oxide by a layer of oleate. The magnetic properties of the nano-objects have been investigated by element specific X-ray magnetic circular dichroism (XMCD) and compared to the properties of the individual components. The heterometallic SMM retains its magnetic properties as part of the hybrid nano-objects due to the oleate SAM that separates the SMM from the magnetic material.

Experimental methods

All reagents were obtained from commercial sources and used-as-received.

Synthesis of $[Co_4Dy(OH)_2(SALOH)_5(chp)_4(MeCN)(H_2O)_2]$ (1): the sample was prepared following the reported experimental procedure.[36]

Synthesis of iron oxide NP:

The synthesis of iron oxide oleate was carried out using the method described in the literature[19]. The synthesis of iron oxide nanoparticles was carried out by modification of a published procedure in the same literature. Iron(III) oleate (2.78 g, 3 mmol), oleic acid (0.96 ml, 3 mmol) and eicosane (10 ml) were mixed in a three-neck round bottom reaction flask and heated to 60 °C, to melt the solvent. Then the reaction mixture was heated to 360 °C, with a heating rate of 3.3 °C/min under stirring and kept refluxing for 10 min and then cooled down to 50 °C. To precipitate the NPs a mixture of 40 ml of acetone and 10 ml of hexane was added to the reaction flask. The NPs were separated by centrifugation and washed three times. For long-term storage, the centrifuged NPs were dispersed in chloroform. NP were characterized by TEM to have a diameter of 8.14±7.38% nm and diffraction expected for Fe_3O_4 (d = 1.487, 2.103, 2.582 and 2.935 Å). SQUID data show Msat/g = 57 emu/g and XMCD pattern (see ESI Figure S4) is in agreement with Fe_3O_4 partially oxidized to Fe_2O_3, as expected for NP this size.[37]

Synthesis of 1-NP:

20 mg of precipitate NPs were shaken with 2 mg of complex **1** and 50 μl of MeOH in chloroform for 48 h. The decorated NPs were magnetically separated and decanted. This action was repeated two more times with chloroform to eliminate the remaining uncoordinated complex.

Characterization techniques

X-Ray diffraction data for complex **1** were already reported by us.[36] The cif file can be obtained free of charge from the Cambridge Structural Database (http://www.ccdc.cam.ac.uk/, deposition number CCDC 1835341)

Elemental analyses (CHN) were performed at Servei de Microanàlisi in CSIC (Consell Superior d'Investigacions Científiques). Infrared spectra were collected on KBr pellets on an AVATAR 330 FT-IR at Departament de Química Inorgànica, Universitat de Barcelona. XPS experiments were performed in a PHI 5500 Multitechnique System (from Physical Electronics) with a monochromatic X-ray source (Aluminium K-alpha line of 1486.6 eV energy and 350 W), placed perpendicular to the analyzer axis and calibrated using the $3d^{5/2}$ line of Ag with a full width at half maximum (FWHM) of 0.8 eV. The analyzed area was a circle of 0.8 mm diameter, and the selected resolution for the spectra was 187.85 eV of pass energy and 0.8 eV/step for the general spectra and 23.5 eV of pass energy and 0.1 eV/step for the spectra of the different elements. A low energy electron gun (less than 10 eV) was used in order to discharge the surface when necessary. All measurements were made in an ultra high vacuum (UHV) chamber at a pressure between $5x10^{-9}$ and $2x10^{-8}$ torr.

Magnetic measurements were performed at the Unitat de Mesures Magnètiques of the Universitat de Barcelona on a Quantum Design SQUID MPMS-XL magnetometer equipped with a 5 T magnet. Diamagnetic corrections for the sample holder and for the sample using Pascal's constants were applied.

Transmission Electron Microscopy: Specimens were analyzed using a JEOL JEM-2100 LaB6 transmission electron microscope with energy dispersed analysis of X-Rays (EDX), operating at 200 kV. The spectrometer is an Oxford Instruments INCA x-sight, with Si (Li) detector,

acquisition was accomplished using the INCA Microanalysis Suite version 4.09 software. Images were recorded with Gatan CCD Camera Orius SC1000 and Digital Micrograph v.1.82.80 software.

XAS and XMCD: The X-ray absorption measurements were performed at the X-Treme beam line[38] at the Swiss Light Source, Paul Scherrer Institut, Switzerland. The X-ray absorption spectra were taken on powder samples pressed into indium foil in total electron yield (TEY) mode. In all measurements, the X-ray beam direction and the magnetic field axis were collinear. Remanence measurements were done after applying either +1 T or -1 T before setting the field to 0 T. In order to avoid damage of the sample and charging effects, the photon flux was reduced to a minimum and a large beam spot with an area of approximately 1 mm^2 was chosen. The degree of circular polarization was virtually 100 %. A number of 10-20 spectra were averaged in order to obtain the XMCD at remanence. Spectra were normalized to the TEY measured simultaneously at a gold mesh located after the exit slit. Furthermore, spectra were normalized to the value at the pre-edge.

Results and discussion

In 2019 we reported a series of new heterometallic SMM of general formulae $[M_4Ln(OH)_2(SALOH)_5(chp)_4(solvent)_3]$ where M = Ni, Co, Ln = Gd, Dy, Tb and La and solvent is either MeOH, MeCN or H_2O using a solvent-free microwave assisted reaction.[36] The cobalt-dysprosium analogue of formula $[Co_4Dy(OH)_2(SALOH)_5(chp)_4(MeCN)(H_2O)_2]$ (**1**) was chosen for this study since it was a low-temperature SMM. Complex **1** contains four hexacoordinated Co(II) ions and one nine-coordinated Dy(III) ion. Detailed crystallographic information can be found in our previous paper.[36] The ligands used have *tert*-butyl groups and chloride-substituted pyridine groups. Figures 1 (a) and (b) show the structure of **1** and a space-filling representation of the four molecules in the unit cell. Figures 1 (c) and (d) show a space-filling representation of complex **1**

with approximate sizes. The size of one molecule of **1** can be obtained from the unit cell dimensions, with 4 molecules in a volume of 12.8 nm^3, each molecule has dimensions of 1.2x1.2x2.0 nm^3. Clearly, one side of the molecule offers a mainly aliphatic surface comprised of the *tert*-butyl groups of the carboxylate ligands, while the other side is highly hydrophobic, dominated by the chlorides of the chp ligands. If the molecule were to lay flat on a surface, its area would be approximately 2.4 nm^2.

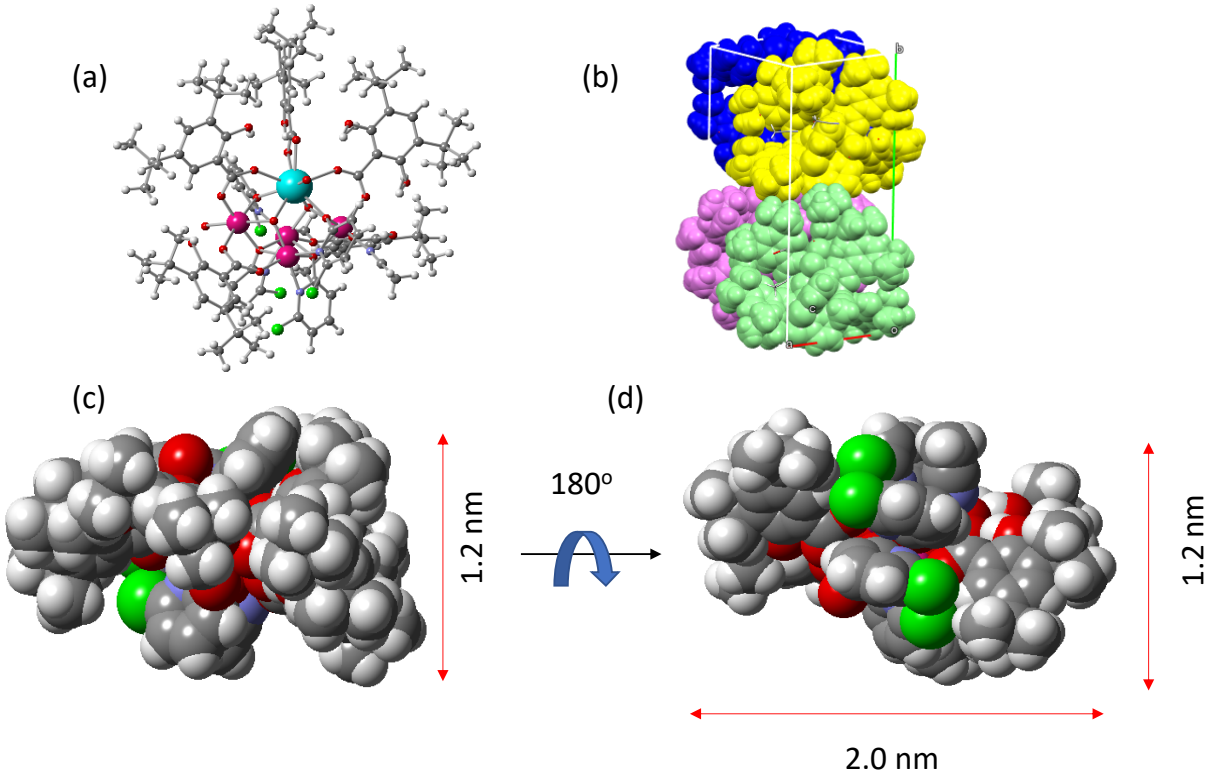

Figure 1. (a) Crystal structure of complex **1**. (b) Space-filling representation of the unit cell of **1** showing each one of the four molecules in different colors. (c) and (d) Space-filling representation of complex **1** with approximate sizes. Color code: C = gray, H = white, Co = dark pink, Dy = cyan, O = red, N = blue, Cl = green (color online).

The detailed experimental and theoretical study of the magnetic properties of complex **1** showed that complex **1** is a low temperature SMM, and that upon application of a dc field of 2000 Oe field-induced SMM properties are observed below 15 K. No hysteresis of the magnetization vs. field was observed for complex **1** at 2 K in a commercial SQUID magnetometer. The magnetic interactions between Co and Dy are ferromagnetic and weak.[36]

Spintronic applications of SMMs and magnetic molecules in general will require the controlled deposition of these molecules on a magnetic surface and a clear understanding of the magnetic interaction between surface and molecule. The surface can be an electrode, in example a metallic electrode, a magnetic electrode or a semiconductor silicon wafer, among others. Carbon based materials can also offer a good surface for molecule deposition.[39] With the aim to study the magnetic interaction between a magnetic surface and a complex molecule like our SMM **1** we chose a simple system, that we had already used: iron oxide nanoparticles (NP) as the magnetic surface[29,40,41] and complex **1** as SMM. The use of iron oxide NP as magnetic surface allows for facile preparation of the hybrid system as well as for the separation and characterization taking advantage of the magnetic character of the NP at room temperature. Previous experiences of studies of the magnetic properties of simple molecules on surfaces show that if the molecule is bound directly on the magnetic material there is strong coupling and the molecular properties cannot be exploited, in particular for transition metal complexes.[42] To mitigate the strong coupling effects, a graphene layer can be used between the nanomagnet and the surface.[43] Alternatively, a thin layer of a diamagnetic material between the surface and the SMM enables the observation of the molecular hysteresis.[8] Following the relevant literature, we decided to use the surfactant of the iron oxide NP as a layer between the magnetic surface and complex **1**. This surfactant is a self-assembled monolayer (SAM) of oleate.[19,23,37] This has clear advantages with respect to other

surfactants, the main one being the possibility to obtain crystalline, monodisperse NP with a SAM of oleate on the surface. In particular, we have used a synthesis adapted from Bronsteins's group[19] that affords iron oxide NP with a SAM of oleate and with sizes between 7 and 20 nm. The NP used in this study had a diameter of 8.14±7.38% nm. The NP were characterized by SQUID magnetometry, TEM, XPS and XAS and XMCD. The TEM images of the **NP** in Figure 2 (a) show regularly shaped crystalline iron oxide NP that are best described as truncated cubes. This fact does not change upon formation of the hybrid system **1-NP** (Figure 2 (b)).

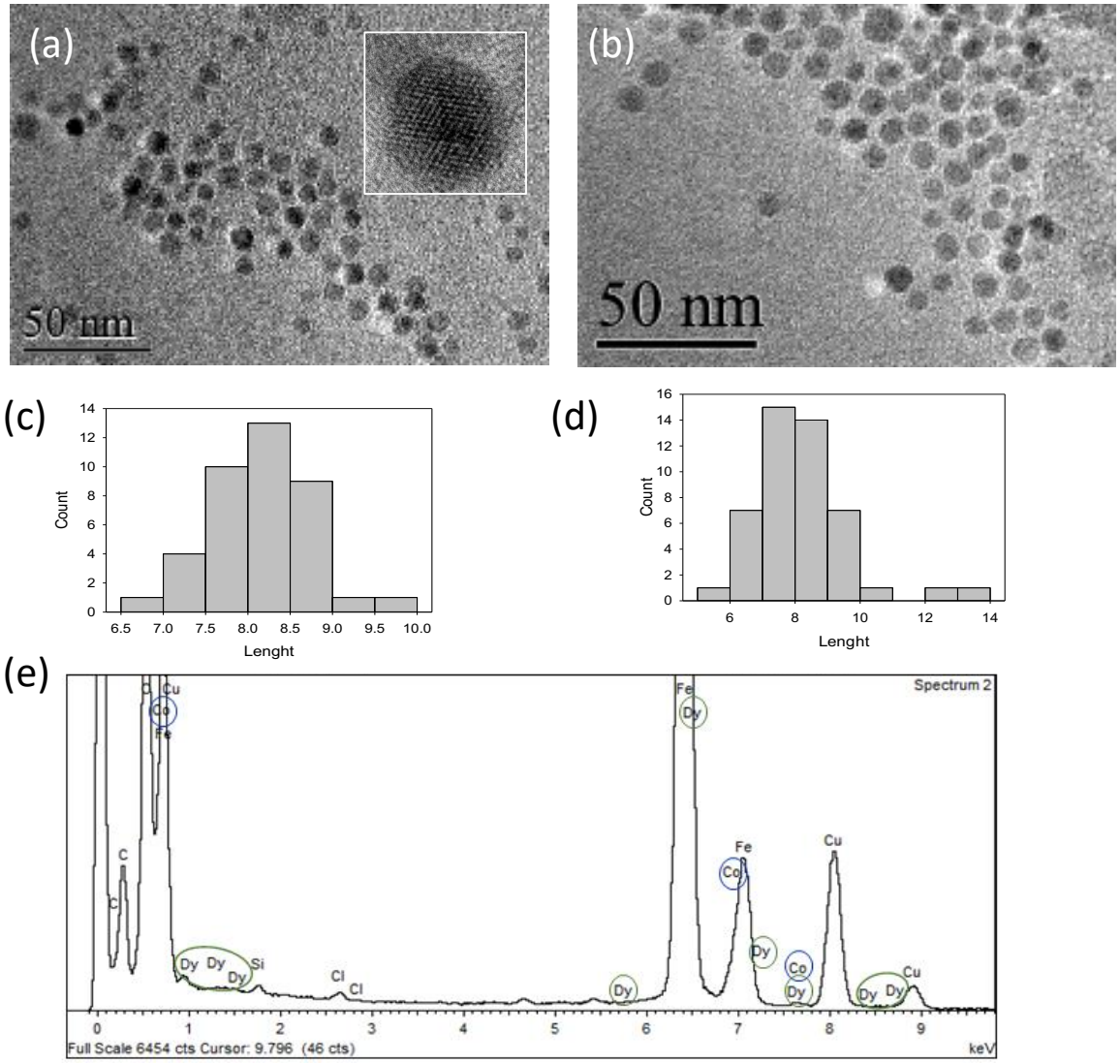

Figure 2. (a) TEM image of iron oxide **NP** with an oleate SAM. The inset shows a high-resolution image of one **NP**. (b) TEM image of iron oxide **1-NP**. (c) Size distribution histogram for **NP**. (d) Size distribution histogram for **1-NP**. (e) EDX analysis for **1-NP**.

The decoration of NP with complex **1** was performed using a very mild method developed in our group.[29,40,41] The NP were magnetically separated and dried. The material was then re-dispersed in 7 mL $CHCl_3$ with 1% MeOH and mixed with 2 mg of complex **1**. The hybrid system **1-NP** was then deposited with a strong magnet, and the solution was decanted. This procedure was repeated three times to wash away unattached material. With this mild functionalization methodology we exploit van-der-Waals interactions between the hydrophobic surface of complex **1** and the exposed aliphatic surface of the SAM of oleate, but we cannot rule out the substitution of some oleate groups by complex **1** molecules.[31] The hybrid system **1-NP** was characterized by TEM, EDX and SQUID magnetometry. TEM images are shown in Figure 2. They show that size, crystallinity and morphology of the NP have not changed in the hybrid system **1-NP**. X-Ray photoemission spectra (XPS) collected for complex **1** (ESI Figure S1), **NP** and the hybrid system **1-NP** reveal the expected peaks for both complex **1** and the iron oxide **NP**. This shows that complex **1** has been attached to the oleate covered iron oxide **NP** to form hybrid nano-objects **1-NP**. Thermogravimetric analysis (TGA) of the NP result in a 12.5% weight loss up to 500°C (ESI Figure S2). This corresponds to the loss of organic matter, that is, the oleate layer. Taking into account the surface area of a sphere model of the nanocrystal of iron oxide, the upper limit for on-surface oleate weight loss is 20%. Thus, the weight loss observed supports the TEM observation that the prepared **NP** are not spherical but have facets and are covered by a SAM of oleate of approximately 500 oleate groups per NP, the SAM of oleate is disrupted on and around the edges

of the nanocrystal. The hybrid system **1-NP** shows a TGA weight loss of 8.5%, thus it is likely that some oleate molecules have been replaced by complex **1** on the surface of the nanocrystal. The TGA loss is in agreement with a coverage of the crystalline **NP** surface by 200-250 oleate groups and 20 molecules of complex **1** in each hybrid **1-NP** nano-object. This number of molecules of complex on each hybrid molecular/inorganic nano-object **1-NP** is in agreement with the surface area of the nanoparticles and the size of one molecule.

SQUID data for both **NP** and **1-NP** are shown in Figure 3 as magnetization (per gram of substance) hysteresis plots.

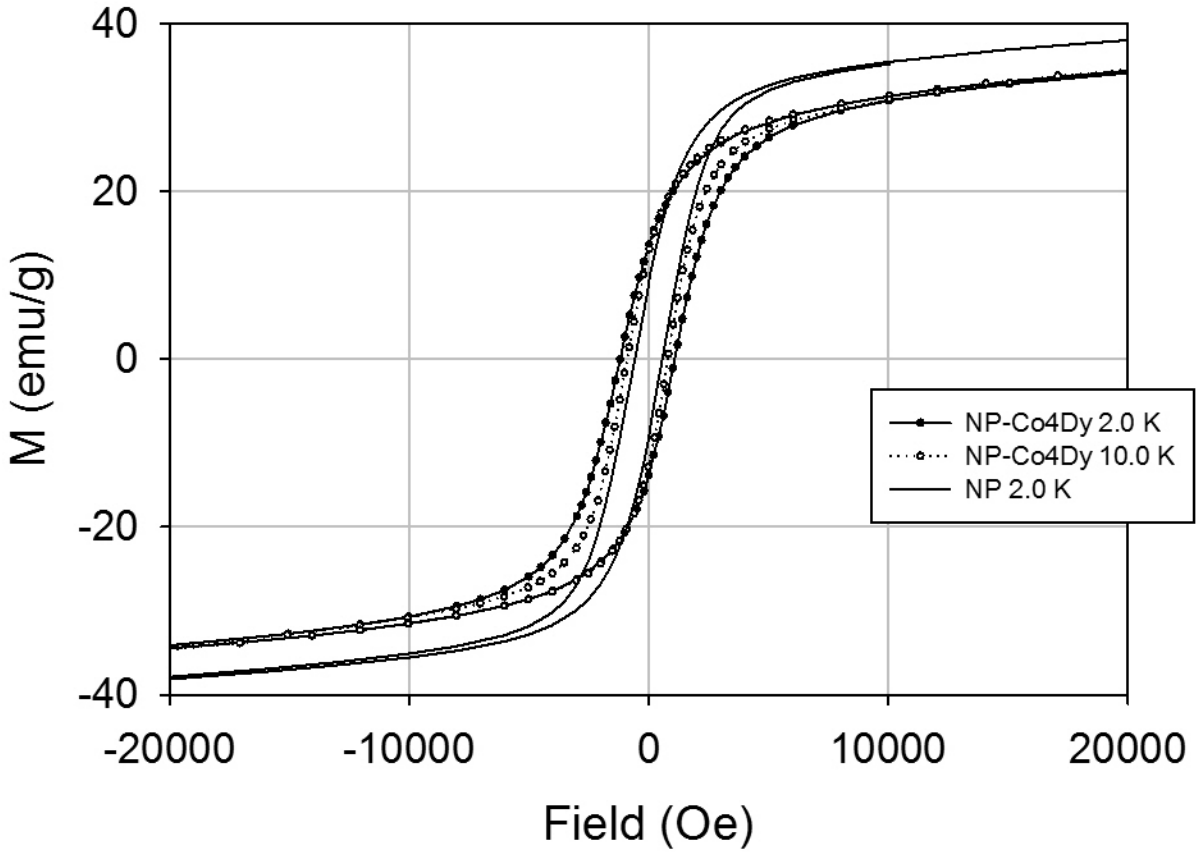

Figure 3. Magnetization vs. field hysteresis plot for **NP** at 2 K and **1-NP** at 2 K and 10 K.

The magnetic data for the hybrid system **1-NP** clearly shows an enhanced hysteresis at 2 K with respect to the hysteresis at the same temperature for the **NP** alone. Clearly, the hysteresis loop of **1-NP** is not the simple sum of the hysteresis curves of **1** and **NP** at 2 K, since complex **1** does not exhibit a magnetic hysteresis opening at 2 K. The coercive field for the oleate covered iron oxide **NP** is 566 Oe at 2 K. The hybrid system **1-NP** has a coercive field of 1144 Oe, with a small negative exchange bias of 67 Oe. This phenomenon has been seen before with SMMs on magnetic surfaces.[29,44,45] The ratio of remanent magnetization vs. saturation magnetization (Mrem/Msat) can give some information regarding inter-particle magnetic coupling. For oleate covered iron oxide **NP** this ratio is 0.20, while for **1-NP** the ratio is 0.33. A Mrem/Msat ratio of 0.5 is expected for non-interacting particles, while smaller values are indicative of antiferromagnetic inter-particle interactions.[46]

In order to further evaluate whether complex **1** was intact in the **1-NP** system and to investigate the contributions to the magnetism by complex **1** and the iron oxide **NP** we used X-ray absorption spectroscopy (XAS) and X-ray magnetic circular dichroism (XMCD). The low-temperature XAS and XMCD obtained in an applied magnetic field on a powder of complex **1** SMMs are shown in Figure 4. Both Co and Dy exhibit a strong magnetic signal. The shape of the Co and Dy spectra is dominated by sharp multiplet features which are in agreement with Co(II) and Dy(III) oxidation states, as expected from structural studies. The sum rule analysis of the Dy spectra (Table S1 and Figure S3) reveals a total magnetic moment of *circa* 4 μ_B per Dy atom at 6.5 T , which is close to the value of 5 μ_B expected for a powder of Dy(III) with strong magnetic anisotropy in saturation. In the case of Co, a sum rule analysis was not performed because of the presence of different Co sites, which cannot be separated in the X-ray spectra. The main XMCD features of both Co and Dy are negative, indicating a magnetic moment oriented along the magnetic field direction. This

suggests either a ferromagnetic coupling of unknown strength of all magnetic ions in complex **1** or a very weak antiferromagnetic coupling which is overruled by the applied magnetic field. Our previous experimental and theoretical study of the magnetic properties of the $[M_4Ln(OH)_2(SALOH)_5(chp)_4(solvent)_3]$ complexes showed that the Dy-Co coupling is small and ferromagnetic.[36]

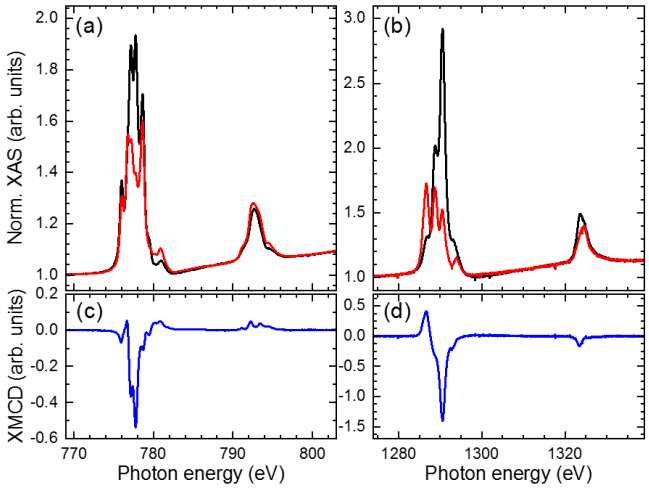

Figure 4. XAS and XMCD of a powder sample of complex **1** recorded at 2 K and 6.5 T at the (a,c) Co $L_{2,3}$ and (b,d) Dy $M_{4,5}$ edges.

The X-ray spectra obtained on the Co and Dy edges on **1-NP**, the SMMs grafted onto the NPs, are shown in Figure 5. Disregarding a lower amount of signal and a change in the background because of the diluted nature of the sample, the main features of the XAS and XMCD spectra remain the same as in the pristine complex **1** sample. This indicates that the SMMs are structurally intact after the grafting process. Some sharp features that were observed on the pristine sample are smeared out in the spectra of the grafted sample, which can be explained by small changes in the Co ligand field originating from different grafting geometries, i.e. orientations of the SMMs on

the oleate SAM-nanoparticles surface. A detailed comparison of the Co L_3 and Dy M_5 edges of the pristine and the grafted SMMs confirms the absence of major changes in the XAS (Figure 5 insets), demonstrating again the intactness of the SMMs on the NPs.

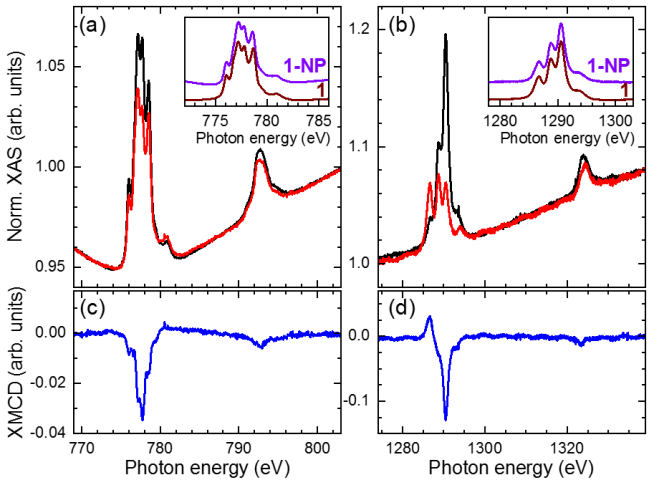

Figure 5. XAS and XMCD of **1-NP** in field at the (a,c) Co $L_{2,3}$ and the (b,d) Dy $M_{4,5}$ edges recorded at 2 K and 6.5 T. Insets in (a,b): Comparison of the normalized XAS obtained at 2 K and 0 T on the pristine SMM **1** and on the hybrid compound **1-NP** as indicated in the plot. Zooms into the (a) Co L_3 edge and the (b) Dy M_5 edges are shown.

Dichroism spectra recorded on the pristine complex **1** and on **1-NP** at different applied magnetic fields and in remanence are depicted in Figure 6. The presence of magnetic remanence in the NPs was independently confirmed (Fig. S4) by recording XMCD at the Fe $L_{2,3}$ edges. The spectra in Figure 6 were normalized to the height of the main Co L_3 XAS feature at an energy of 777.2 eV. First we focus on the Co spectra shown in Fig. 6a. Clearly the XMCD signal, which is proportional to the Co total magnetic moment, is significantly weaker in the grafted sample compared to the pristine one. This is possibly due to a modification of the intramolecular exchange coupling paths upon grafting.

In order to obtain information about the magnetic coupling between SMMs and NPs it is useful to investigate the remanent behavior. In **1-NP** in the presence of SMM-NP magnetic coupling and at low enough temperatures, the coupled SMMs should follow the remanence of the NPs. In particular, the induced remanent magnetic moment of the SMMs should show a sign flip when the remanence condition is approached from a positive or from a negative applied magnetic field. The XMCD spectra taken at remanence at the Co L_3 edge indeed are non-zero and for the case of the grafted SMMs in **1-NP** they flip their sign depending on the sign of the field applied to the sample prior to the remanence measurement. From the amplitude of the strongest XMCD feature, averaged over the (+) and (-) remanence condition, and from the one observed at 0.5 T, an upper bound for the effective magnetic field seen by the SMMs can be obtained. More precisely,

$$B_{\mathrm{eff,max}} = \frac{\max\left(\left|\mathrm{XMCD}(E)^{+0.0} - \mathrm{XMCD}(E)^{-0.0}\right|\right)}{2\ \max\left(\left|\mathrm{XMCD}(E)^{+0.5}\right|\right)} \times 0.5\ \mathrm{T} \quad \text{(Eq. 1)}$$

When applying Eq.(1) to the cases of the pristine complex **1** and of the grafted SMMs in **1-NP**, respectively, we obtain upper bounds of $B_{eff,max}$ = 33 mT for the pristine SMMs and 110 mT for the grafted SMMs. The difference can be understood by the slightly larger remanent signals combined with the smaller susceptibility of the grafted SMMs. While the $B_{eff,max}$ of the pristine SMM sample comes close to the remanent field of the superconducting magnet used to apply the external field, which is on the order of 10 mT, the larger effective field seen by the grafted SMMs could be originating from a small magnetic coupling between SMMs and NPs. Nevertheless, the effective field and thus the coupling of dipolar or exchange nature, if it exists, is very small. Comparison of the XMCD spectral shape of the grafted SMMs in remanence with the one measured in applied field, as well as comparing with the pristine SMMs in remanence, suggests that the SMM-NP coupling is antiferromagnetic.

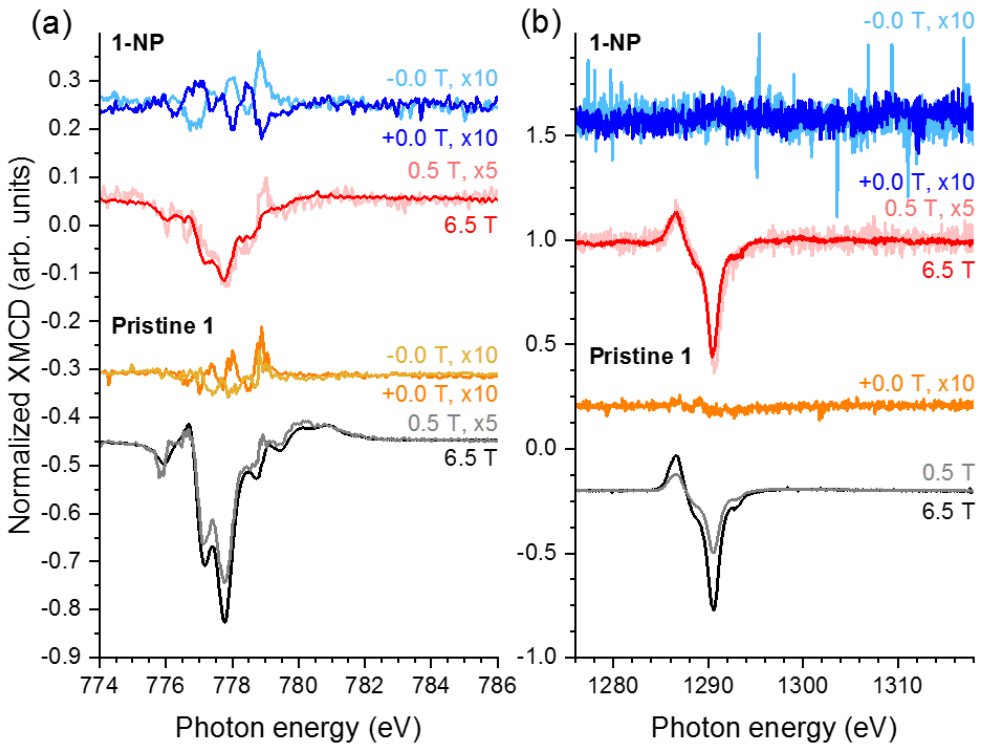

Figure 6. Comparison of XMCD recorded at 2 K for **1** and **1-NP** at the (a) Co L_3 and the (b) Dy M_5 edges in remanence and at different applied fields as indicated in the plots.

In the case of Dy as shown in Figure 6b, clearly no sign of remanence is detected, despite the presence of a few electronic glitches. The field dependence of the XMCD in the pristine **1** is different for Dy and Co, in that Dy shows a stronger dependence. The field dependence of Dy in **1-NP** is similar to the one observed for Co, which could be ascribed to a stronger Dy-Co coupling **1-NP**, originating from structural changes in the grafting process.

The XMCD data suggest a favored orientation of the SMM **1** in which the Co(II) ions are closer to the iron oxide: this coincides with the hydrophobic face exposing the chlorine atoms of chp ligands (see Figure 1). However, one must consider the possibility of a distribution of distances between iron oxide NP and SMM due to different dispositions of the SMM on the SAM of oleate

or directly on the NP surface, thus there is a distribution of fields felt by the molecules. The typical dipolar field for a 5 nm iron oxide NP has been calculated by Moya and co-workers as 114 Oe (11.4 mT) at a distance of 1 nm from the iron oxide.[47] Larger values can be expected in the present system that are consistent with the calculated upper bound for the effective magnetic field seen by the SMMs as calculated form XMCD (110 mT). The fact that this calculated effective field is one order of magnitude larger could be caused by the SMMs being closer to the iron oxide. This fact could be consistent with molecules of complex **1** being embedded in the oleate SAM or to the exchange of complex **1** and oleate, as TGA data suggest.

The hysteresis enhancement observed for the hybrid **1-NP** system when compared to the pristine **NP** cannot be attributed to a strong coupling between the SMM **1** and the iron oxide **NP**, as XMCD shows that there is no clear magnetic coupling. However, the shell of oleate/SMMs is highly anisotropic and this is a key point. The anisotropic shell of SMMs is thus affecting the hybrid system hysteresis by enhancing the hysteretic behavior of iron oxide **NP**s.

Conclusions

The heterometallic Co_4Dy SMM **1**, has been deposited on to iron oxide **NP** using a mild and facile method. The obtained hybrid molecular-inorganic nano-objects **1-NP** have been thoroughly characterized as monodisperse, crystalline iron oxide **NP** with a SAM of oleate decorated with complex **1** SMMs. X-ray absorption spectroscopy reveals that the deposited SMMs are structurally intact, and the XMCD characterization of the sample proves that complex **1** retains its magnetic properties on the surface of the magnetic substrate functionalized with oleate. Furthermore, there is only weak coupling between the Co(II) ions and the iron oxide. Thus, an organic SAM, in this case an oleate layer, between the iron oxide **NP** and complex **1** plays a key role in ensuring that

there is no strong magnetic coupling between the magnetic surface and the SMM. The lack of remanence in XMCD for the Dy ions indicates a preferential orientation of complex **1** on the substrate, that coincides with a very hydrophobic face exposing chlorine atoms of chp ligands. The oleate SAM allows for the complex to interact by weak van–der-Waals interactions with the substrate, and at the same time it avoids strong coupling between magnetic substrate and SMM. The anisotropic shell of SMMs enhances the hysteretic behavior of iron oxide **NP**s, and this could be exploited for a variety of applications of magnetic NPs. The nano-objects reported here contain a limited number of molecules, with defined sizes and that can be easily manipulated. In this regard, one could use this hybrid system to address a small number of SMMs on an easy-to-manipulate nano-object. Molecular spintronic applications require that SMMs remain intact and retain their magnetic properties when deposited on a substrate. The use of organic spacers is not widespread, but it is understood that the decoupling between the magnetic surface and the SMM is a key factor, great success in this regard has been reported with the use of inorganic materials like MgO[8] or graphene[48] between the SMM and a metallic or magnetic surfaces. We show here that this can be easily achieved using an organic spacer between SMM and magnetic surface. We are now working to extend our approach to flat surfaces like semiconductors or metals. In these systems we intend to study the robustness of the organic spacer layer.

ASSOCIATED CONTENT

Supporting Information available as ESI.pdf file.

AUTHOR INFORMATION

Corresponding Author

*email: esanudo@ub.edu

Author Contributions

The manuscript was written through contributions of all authors. All authors have given approval to the final version of the manuscript. ‡

Funding Sources

Spanish Government Ministerio de Economía y Competitividad via Feder Funds (Grant CTQ2015-68370-P and PGC2018-098630-B-I00).

ACKNOWLEDGMENT

We acknowledge Zhanna Kenzhalina for assistance with the X-ray measurements. LRP, ECS acknowledge the financial support of the Spanish Government Ministerio de Economía y Competitividad via Feder Funds (CTQ2015-68370-P and PGC2018-098630-B-I00).

SYNOPSIS (Word Style "SN_Synopsis_TOC"). If you are submitting your paper to a journal that requires a synopsis, see the journal's Instructions for Authors for details.

REFERENCES

1 R. Sessoli, H.-L. Tsai, A. R. Schake, S. Wang, J. B. Vincent, K. Folting, D. Gatteschi, G. Christou and D. N. Hendrickson, High-Spin Molecules:[Mn12Ol2(O2CR)16(H2O)4], *J. Am. Chem. Soc.*, 1993, **115**, 1804–1816.

2 H. J. Eppley, H. T. Nadine, K. Felting, G. Christou and D. N. Hendrickson, High-Spin Molecules : Unusual Magnetic Susceptibility Relaxation Effects in [Mn12O12(O2CEt)16(H2O)3] (S=9) and the One-Electron Reduction Product (PPh4)[Mn12O12(O2CEt)16(H2O)4] (S=19/2), *J. Am. Chem. Soc.*, 1995, **117**, 301–317.

3 L. Rosado Piquer and E. C. Sañudo, Heterometallic 3d–4f single-molecule magnets, *Dalt. Trans.*, 2015, **44**, 8771–8780.

4 J. D. Rinehart and J. R. Long, Exploiting single-ion anisotropy in the design of f-element single-molecule magnets, *Chem. Sci.*, 2011, **2**, 2078–2085.

5 D. N. Woodruff, R. E. P. Winpenny and R. A. Layfield, Lanthanide single-molecule magnets., *Chem. Rev.*, 2013, **113**, 5110–5148.

6 N. Ishikawa, M. Sugita and W. Wernsdorfer, Quantum tunneling of magnetization in lanthanide single-molecule magnets: bis(phthalocyaninato)terbium and bis(phthalocyaninato)dysprosium anions., *Angew. Chem. Int. Ed. Engl.*, 2005, **44**, 2931–5.

7 N. Ishikawa, M. Sugita, T. Ishikawa, S.-Y. Koshihara and Y. Kaizu, Lanthanide double-decker complexes functioning as magnets at the single-molecular level., *J. Am. Chem. Soc.*, 2003, **125**, 8694–8695.

8 C. Wäckerlin, F. Donati, A. Singha, R. Baltic, S. Rusponi, K. Diller, F. Patthey, M. Pivetta, Y. Lan, S. Klyatskaya, M. Ruben, H. Brune and J. Dreiser, Giant Hysteresis of Single-Molecule Magnets Adsorbed on a Nonmagnetic Insulator, *Adv. Mater.*, 2016, **28**, 5195–5199.

9 S. a Sulway, R. a Layfield, F. Tuna, W. Wernsdorfer and R. E. P. Winpenny, Single-

molecule magnetism in cyclopentadienyl-dysprosium chlorides., *Chem. Commun. (Camb).*, 2012, **48**, 1508–10.

10 T. Pugh, F. Tuna, L. Ungur, D. Collison, E. J. L. McInnes, L. F. Chibotaru and R. A. Layfield, Influencing the properties of dysprosium single-molecule magnets with phosphorus donor ligands, *Nat. Commun.*, 2015, **6**, 7492.

11 F. S. Guo, B. M. Day, Y. C. Chen, M. L. Tong, A. Mansikkamäki and R. A. Layfield, A Dysprosium Metallocene Single-Molecule Magnet Functioning at the Axial Limit, *Angew. Chemie - Int. Ed.*, 2017, **56**, 11445–11449.

12 F. Guo, B. M. Day, Y. Chen, M. Tong, A. Mansikkamäki and R. A. Layfield, Magnetic hysteresis up to 80 kelvin in a dysprosium metallocene single-molecule magnet, *Science (80-.).*, 2018, **362**, 1400–1403.

13 C. A. P. Goodwin, F. Ortu, D. Reta, N. F. Chilton and D. P. Mills, Molecular magnetic hysteresis at 60 kelvin in dysprosocenium, *Nature*, 2017, **548**, 439–442.

14 R. Sessoli, Magnetic molecules back in the race, *Nature*, 2017, **548**, 400–401.

15 G. Cosquer, F. Pointillart, S. Golhen, O. Cador and L. Ouahab, Slow magnetic relaxation in condensed versus dispersed dysprosium(III) mononuclear complexes, *Chem. - A Eur. J.*, 2013, **19**, 7895–7903.

16 F. Habib, P. Lin, J. Long, I. Korobkov, W. Wernsdorfer and M. Murugesu, The Use of Magnetic Dilution To Elucidate the Slow Magnetic, *J. Am. Chem. Soc.*, 2011, **133**, 8830–8833.

17 L. Vergnani, A.-L. Barra, P. Neugebauer, M. J. Rodriguez-Douton, R. Sessoli, L. Sorace, W. Wernsdorfer and A. Cornia, Magnetic bistability of isolated giant-spin centers in a diamagnetic crystalline matrix., *Chemistry*, 2012, **18**, 3390–8.

18 J. M. Zadrozny and J. R. Long, Slow magnetic relaxation at zero field in the tetrahedral complex [Co(SPh)4]2-., *J. Am. Chem. Soc.*, 2011, **133**, 20732–4.

19 L. M. Bronstein, X. Huang, J. Retrum, A. Schmucker, M. Pink, B. D. Stein and B. Dragnea, Influence of iron oleate complex structure on iron oxide nanoparticle formation, *Chem. Mater.*, 2007, **19**, 3624–3632.

20 Q. A. Pankhurst, J. Connolly, S. K. Jones and J. Dobson, Applications of magnetic nanoparticles in biomedicine, *J. Phys. D. Appl. Phys.*, 2003, **36**, R167–R181.

21 A. G. Kolhatkar, A. C. Jamison, D. Litvinov, R. C. Willson and T. R. Lee, Tuning the magnetic properties of nanoparticles., *Int. J. Mol. Sci.*, 2013, **14**, 15977–6009.

22 S. Singamaneni, V. N. Bliznyuk, C. Binek and E. Y. Tsymbal, Magnetic nanoparticles: recent advances in synthesis, self-assembly and applications, *J. Mater. Chem.*, 2011, **21**, 16819.

23 A. Lu, E. L. Salabas and F. Schüth, Magnetic Nanoparticles : Synthesis, Protection, Functionalization and Application, *Angew. Chemie, Int. Ed.*, 2007, **46**, 1222–1244.

24 A. D. Oberdick, A. M. Abdelgawad, C. Moya, S. Mesbahi-Vasey, D. Kepaptsoglou, V. K. Lazarov, R. F. L. Evans, D. Meilak, E. Skoropata, J. V. Lierop, I. Hunt-Isaak, H. Pan, Y. Ijiri, K. L. Krycka, J. A. Borchers and S. A. Majetich, Spin canting across core/shell Fe3O4/MnxFe3-xO4 nanoparticles, *Sci. Rep.*, 2017, **Accepted**, 1–12.

25 J.-H. Lee, J.-T. Jang, J.-S. Choi, S. H. Moon, S.-H. Noh, J.-G. J.-W. J.-G. J.-W. Kim, J.-G. J.-W. J.-G. J.-W. Kim, I.-S. Kim, K. I. Park and J. Cheon, Exchange-coupled magnetic nanoparticles for efficient heat induction., *Nat. Nanotechnol.*, 2011, **6**, 418–422.

26 S. H. Moon, S. H. Noh, J. H. Lee, T. H. Shin, Y. Lim and J. Cheon, Ultrathin Interface Regime of Core-Shell Magnetic Nanoparticles for Effective Magnetism Tailoring, *Nano Lett.*, 2017, **17**, 800–804.

27 E. A. Kwizera, E. Chaffin, Y. Wang and X. Huang, Synthesis and properties of magnetic-optical core–shell nanoparticles, *RSC Adv.*, 2017, **7**, 17137–17153.

28 F. Magnus, M. E. Brooks-Bartlett, R. Moubah, R. A. Procter, G. Andersson, T. P. A. Hase, S. T. Banks and B. Hjörvarsson, Long-Range magnetic interactions and proximity effects in an amorphous exchange-spring magnet, *Nat. Commun.*, 2016, **7**, 1–7.

29 L. Rosado Piquer, E. Jiménez, Y. Lan, W. Wernsdorfer, G. Aromi and E. C. Sañudo, Hybrid molecular-inorganic materials: Heterometallic [Ni4Tb] complex grafted on superparamagnetic iron oxide nanoparticles, *Inorg. Chem. Front.*, 2017, **4**, 595–603.

30 L. Rosado Piquer, M. Escoda-Torroella, M. Ledezma Gairaud, S. Carneros, N. Daffé, M. Studniarek, J. Dreiser, W. Wernsdorfer and E. Carolina Sañudo, Hysteresis enhancement on a hybrid Dy(iii) single molecule magnet/iron oxide nanoparticle system, *Inorg. Chem. Front.*, 2019, **6**, 705–714.

31 L. R. Piquer, R. R. Sánchez, E. C. Sañudo and J. Echeverría, Understanding the molecule-electrode interface for molecular spintronic devices: A computational and experimental study, *Molecules*, , DOI:10.3390/molecules23061441.

32 R. J. Holmberg, A. J. Hutchings, F. Habib, I. Korobkov, J. C. Scaiano and M. Murugesu, Hybrid Nanomaterials : Anchoring Magnetic Molecules on Naked Gold Nanocrystals, *Inorg. Chem.*, 2013, **52**, 14411–14418.

33 D. Mitcov, A. H. Pedersen, M. Ceccato, R. M. Gelardi, T. Hassenkam, A. Konstantatos, A. Reinholdt, A. Rogalev, W. Wernsdorfer, E. K. Brechin and S. Piligkos, Molecular multifunctionality preservation upon surface deposition for a chiral single-molecule magnet †, *Chem. Sci.*, 2019, **10**, 3065–3073.

34 M. Perfetti, F. Pineider, L. Poggini, E. Otero, M. Mannini, L. Sorace, C. Sangregorio, A. Cornia and R. Sessoli, Grafting single molecule magnets on gold nanoparticles, *Small*, 2014, **10**, 323–329.

35 Y. Prado, N. Daffé, A. Michel, T. Georgelin, N. Yaacoub, J. M. Grenèche, F. Choueikani, E. Otero, P. Ohresser, M. A. Arrio, C. Cartier-Dit-Moulin, P. Sainctavit, B. Fleury, V. Dupuis, L. Lisnard and J. Fresnais, Enhancing the magnetic anisotropy of maghemite nanoparticles via the surface coordination of molecular complexes, *Nat. Commun.*, 2015, **6**, 10139.

36 L. R. Piquer, S. Dey, S. J. Teat, J. Cirera, G. Rajaraman and E. C. Sañudo, Microwave assisted synthesis of heterometallic 3d–4f M4Ln complexes, *Dalt. Trans.*, 2019, **48**, 12440–12450.

37 J. Park, K. An, Y. Hwang, J. Park, H. Noh, J. Kim, J. Park, N. Hwang and T. Hyeon, Ultra-large-scale syntheses of monodisperse nanocrystals, *Nat. Mater.*, 2004, **3**, 891–895.

38 C. Piamonteze, U. Flechsig, S. Rusponi, J. Dreiser, J. Heidler, M. Schmidt, R. Wetter, M.

Calvi, T. Schmidt, H. Pruchova, J. Krempasky, C. Quitmann, H. Brune and F. Nolting, X-Treme beamline at SLS: X-ray magnetic circular and linear dichroism at high field and low temperature, *J. Synchrotron Radiat.*, 2012, **19**, 661–674.

39 M. J. Heras Ojea, D. Reta Mañeru, L. Rosado, J. Rubio Zuazo, G. R. Castro, S. Tewary, G. Rajaraman, G. Aromí, E. Jiménez and E. C. Sañudo, Characterization of a robust Co(II) fluorescent complex deposited intact on HOPG, *Chem. - A Eur. J.*, 2014, **20**, 10439–10445.

40 L. Rosado Piquer, R. Royo Sánchez, E. C. Sañudo and J. Echeverrerría, Understanding the Molecule-Electrode Interface for Molecular Spintronic Devices : A Computational and Experimental Study, *Molecules*, 2018, **23**, 1441–1456.

41 L. Rosado Piquer, M. Escoda-Torroella, M. Ledezma Gairaud, S. Carneros, N. Daffé, M. Studniarek, W. Wernsdorfer, J. Dreiser and E. C. Sañudo, Hysteresis enhancement on a hybrid Dy(iii) single molecule magnet/iron oxide nanoparticle system, *Inorg. Chem. Front.*, 2019, **6**, 705–714.

42 A. Lodi Rizzini, C. Krull, T. Balashov, J. J. Kavich, A. Mugarza, P. S. Miedema, P. K. Thakur, V. Sessi, S. Klyatskaya, M. Ruben, S. Stepanow and P. Gambardella, Coupling Single Molecule Magnets to Ferromagnetic Substrates, *Phys. Rev. Lett.*, 2011, **107**, 177205.

43 G. Avvisati, C. Cardoso, D. Varsano, A. Ferretti, P. Gargiani and M. G. Betti, Ferromagnetic and Antiferromagnetic Coupling of Spin Molecular Interfaces with High Thermal Stability, *Nano Lett.*, 2018, **18**, 2268–2273.

44 C. Nistor, C. Krull, A. Mugarza, S. Stepanow, C. Stamm, M. Soares, S. Klyatskaya, M. Ruben and P. Gambardella, Exchange bias of TbPc 2 molecular magnets on

antiferromagnetic FeMn and ferromagnetic Fe films, *Phys. Rev. B*, 2015, **92**, 184402.

45 A. L. Rizzini, C. Krull, T. Balashov, A. Mugarza, C. Nistor, F. Yakhou, V. Sessi, S. Klyatskaya, M. Ruben, S. Stepanow and P. Gambardella, Exchange Biasing Single Molecule Magnets: Coupling of TbPc 2 to Antiferromagnetic Layers, *Nano Lett.*, 2012, 5703–5707.

46 G. F. Goya, T. S. Berquó, F. C. Fonseca and M. P. Morales, Static and dynamic magnetic properties of spherical magnetite nanoparticles, *J. Appl. Phys.*, 2003, **94**, 3520–3528.

47 C. Moya, Ó. Iglesias, X. Batlle and A. Labarta, Quantification of dipolar interactions in Fe 3-x O 4 nanoparticles, *J. Phys. Chem. C*, 2015, **119**, 24142–24148.

48 V. Corradini, A. Candini, D. Klar, R. Biagi, V. De Renzi, A. Lodi Rizzini, N. Cavani, U. Del Pennino, S. Klyatskaya, M. Ruben, E. Velez-Fort, K. Kummer, N. B. Brookes, P. Gargiani, H. Wende and M. Affronte, Probing magnetic coupling between LnPc2 (Ln = Tb, Er) molecules and the graphene/Ni (111) substrate with and without Au-intercalation: Role of the dipolar field, *Nanoscale*, 2018, **10**, 277–283.